



Transport and reaction phenomena in multilayer membranes functioning as bioartificial kidney devices



R. Refoyo^a, E.D. Skouras^a, N.V. Chevtchik^b, D. Stamatialis^b, V.N. Burganos^{a,*}

^a Institute of Chemical Engineering Sciences, Foundation for Research and Technology, Hellas, (FORTH/ICE-HT), Greece

^b (Bio)artificial organs, Department of Biomaterials Science and Technology, Faculty of Science and Technology, TechMed Institute, University of Twente, The Netherlands

ARTICLE INFO

Keywords:

Hollow fiber membrane
Protein-bound uremic toxins
Bioartificial kidney device
Cell monolayer modeling
Organic ion transporters

ABSTRACT

Classic hemodialysis only provides a limited removal of protein bound uremic toxins (PBUT) in patients with chronic kidney disease. A bioartificial kidney device, BAK, composed of a living cell monolayer of conditionally immortalized proximal tubule epithelial kidney cells (ciPTEC) cultured of hollow fiber polymeric membrane can remove protein bound uremic toxins from the blood in combination with classic hemodialysis. The development and clinical implementation of the BAK requires lots of optimization. This investigation is expensive and time consuming therefore modeling studies could help to optimize experiments and improve its design.

In this work, a 3D mathematical model of the BAK is developed. The transport and reaction mechanisms associated with the removal of PBUT indoxyl sulfate are considered and various conditions are simulated. The model describes a single hollow fiber membrane and considers different domains for the blood flow, the membrane, the cell monolayer, and the dialysate region. A mathematical description of the relevant transport and/or reaction mechanisms is provided in each domain, and the corresponding differential equations are solved numerically. Since not all the modeling constants are experimentally available, a parametric study is performed for their quantification, including the active transport kinetics of the toxins through the cell monolayer, in comparison to the passive transport rates by diffusion. The parametric study also provides a background for the extraction of usually unknown quantities, including notably the Organic Anion Transporter (OAT) concentrations, with the support of experimental data. Satisfactory reproduction of experimental findings is achieved, and the role of systemic variables that affect significantly the uremic toxin removal is identified.

1. Introduction

For patients with end stage kidney disease (ESKD) the best solution currently is organ transplantation. However, not all patients are eligible for transplantation and, due to limited organ availability, most patients are currently treated with dialysis (such as peritoneal or hemodialysis), which only covers a small part of the kidney function. In the natural kidney, the nephron achieves complete solute removal by the combined action of glomerular and tubule filtrations. Small toxins are filtrated through glomerulus whereas larger and protein bound uremic toxins are removed by the active filtration of the proximal tubule. Hemodialysis, in fact, only mimics the action of the glomerulus removing only small water-soluble toxins, and partly the middle molecules. However, it cannot remove protein-bound uremic toxins to a satisfactory degree that would prevent accumulation of these toxins and evidently to considerable morbidity and mortality rates [1,2].

An alternative solution to achieve improved removal of free and

protein-bound uremic toxins is an apt combination of classic hemodialysis with a bioartificial kidney device [3–8]. Its primary component is a hybrid living membrane; namely, a hollow fiber polymeric membrane [5] coated with human collagen IV and L-Dopamine, where a monolayer of immortalized living proximal tubule epithelial kidney cells (ciPTEC) [9] is attached. This cell layer contributes to the active removal of protein-bound toxins through the combined action of organic ion transporters (OAT), present in the basolateral surface of the cell, and the efflux pump transporters breast cancer resistant protein (BCRP) and multidrug resistance protein-4 (MRP4), both of them present in the apical surface of the cell. In the case of indoxyl sulfate the specific basolateral transporter is organic anion transporter 1 (OAT1) [10,11].

Several experiments have already demonstrated the successful formation of a tight cell monolayer with the expression of organic ionic transporters both in flat and in hollow fiber membranes [9,12–14]. Computer simulations [15–17] can facilitate the optimization of the

* Corresponding author.

E-mail address: vbur@iceht.forth.gr (V.N. Burganos).

<https://doi.org/10.1016/j.memsci.2018.08.007>

Received 2 May 2018; Received in revised form 5 July 2018; Accepted 6 August 2018

Available online 07 August 2018

0376-7388/ © 2018 Elsevier B.V. All rights reserved.

Nomenclature

BAK	Bioartificial kidney device
BCRP	Breast cancer resistant protein
ciPTEC	Immortalized proximal tubule epithelial cells
MRP4	Multidrug resistance protein-4
OIT	Organic ion transporters
OCT2	Organic cation transporter 2
OAT1	Organic anion transporter 1
PBUT	Protein-bound uremic toxin
HSA	Human Serum Albumin
C_i	Toxin i
D_i	Diffusion coefficient [m^2/s]
$R_{i,b}$	Binding reaction rate [$\text{mol}/\text{m}^3 \text{ s}$]
$N_{i,1}$	Prefactor of binding kinetics [dimensionless]
$K_{i,1}$	Binding constant [m^3/mol]

C_i	Toxin local concentration [mol/m^3]
C_{HSA}	Albumin local concentration [mol/m^3]
$C_{\text{HSA}i}$	Albumin-toxin i local concentration [mol/m^3]
ε	Membrane porosity [dimensionless]
τ	Membrane tortuosity [dimensionless]
u_z	Local linear velocity [m/s]
C_{is}	Toxin local surface concentration [mol/m^3]
R_{OAT}	Michaelis-Menten reaction rate for the OATs transport [$\text{mol}/\text{m}^3 \text{ s}$]
V_{MAX}	Maximum MM reaction rate, [$\text{nmol}/\text{mg}_{\text{protein}} \text{ min}$]
K_M	MM constant [$\mu\text{mol}/\text{L}$]
Cl_i	Clearance [$\mu\text{L}/\text{min cm}^2$]
S	Surface [m^2]
R	Radius [μm]
L	Length [mm]

design of new experiments and devices through the characterization of the behavior of the cell monolayer under various conditions.

In the present work, the transport phenomena and the different mechanisms that are involved in the removal of a protein bound uremic toxin, namely, of the indoxyl sulfate, IS, from the blood are investigated, as offered by a single hollow fiber membrane with an attached living ciPTEC cell monolayer. The main goals involve the quantification of the role of this layer, the study of the key transport and reaction mechanisms that are involved, and the investigation of the effect of the major process parameters on the toxin clearance, with the eventual aim to guide further improvement of the toxin removal process with the help of experimental data which eventually leads to the design of better BAK devices. A typical bioreactor is composed of a bundle of roughly 1000 fibers with a length of 10 cm distributed in parallel. If the fibers are evenly separated from each other, it is usually assumed that fiber interaction can be effectively averaged at the scale of a single fiber, thus allowing extrapolation of the results to the whole bioreactor. A 3D mathematical model of a single hollow fiber with a cell monolayer is constructed here. Toxin IS [18] has a 75–95% bound fraction to Human Serum Albumin (HSA) under normal conditions. The model was used for the simulation of experimental processes of transcellular transport of toxins in BAK devices [12,14], where performance data in the form of toxin clearances were extracted and used for the fitting of the modeling parameters.

2. Model development

The details of the model that describes toxin removal through a hollow fiber equipped with a cell monolayer are presented in this section. The model presented here is built with the inside-out configuration; the blood flows in the lumen of the membrane whereas the cell monolayer is attached on the outside surface of the fiber in contact with the dialysate. The model can also be built with the outside-in configuration, in which the blood or the blood plasma flows on the outside of the hollow fiber membrane and the cell monolayer is attached to the inner part of the membrane in direct contact with a dialysate which, depending on the type of the process, can be either flowing, or stagnant. In the outside-in configuration, clogging of the blood is avoided [19] but the inside-out configuration facilitates seeding of the cell monolayer on the hollow fiber membrane and is the one that is considered in the present work.

The model domain is divided into four distinct subdomains and offers a mathematical description of all relevant transport and reaction mechanisms in each one. Specifically, the domains and the corresponding mechanisms are: The blood domain, where diffusion, convection, and binding kinetics of IS to HSA [20] are considered; the porous membrane domain, where diffusion and binding kinetics are

considered; the cell monolayer domain, where Michaelis-Menten transport reaction is assumed at their membrane walls [11] to describe toxin-cell interaction, and diffusion is the main mechanism of bulk transport within; the urine domain, where diffusion is also the sole mechanism of transport.

In order to simulate the effect of the IS transport by the organic transporters, a Michaelis-Menten model is implemented. With this model, the toxin flux on the interface wall between the porous membrane and the basolateral side of the cell is assumed to be given by a Michaelis-Menten surface uptake expression. On the apical side of the cell domain, flux continuity is employed as boundary condition. Finally, in the dialysate domain, diffusion is the only mechanism considered, due to the stagnant form of the dialysate used in the respective experiments [12].

Fig. 1(a) illustrates the structure and the dimensions of the model and Fig. 1(b) shows the configuration of the different domains of the model and the streams. The ciPTECs are genetically engineered so they can proliferate at 33 °C and differentiate and remain stable at 37 °C once the cell monolayer is formed. Accordingly, the process can be assumed isothermal, with no change in the cell density, no cell differentiation or death, and no fiber degradation. The cell monolayer usually receives oxygen and nutrients by direct absorption from the dialysate site, which is also the cell culture medium, without transport restrictions. In the present model it is assumed that the oxygen and the nutrients do not interfere with the toxins and, thus, they do not pose any limiting factors to either transport or reactivity. Hence, supply and transport of oxygen and nutrients are not considered in this model.

Based on the symmetry of the hollow fiber membrane, the model can be fully formulated in cylindrical coordinates. Convection is dominant in the longitudinal direction of the fiber, however both diffusion and convection are considered in the transport equation; fully-developed laminar blood/plasma flow is assumed over the length of the fiber. Along the flow direction, the membrane geometry is invariant. The flow and transport equations in every subdomain are described with appropriate boundary conditions at the interfaces between successive compartments.

The blood domain corresponds to the inner part of the hollow fiber. In this region, the water properties are adopted for the density and the viscosity of the human blood plasma, and to express the diffusivities of the toxins. The choice of water properties was based on the fact that most of the pertinent experiments [12] were carried out with an aqueous buffer solution. This choice is also a conventional assumption that is typically implemented during modeling of laboratory experiments that employ aqueous solutions instead of human plasma. In any case, for the sake of comparison, the base-case simulations were repeated using the viscosity of the blood, which is *ca* 4 times higher than that of water at 37 °C. If required, more detailed description of the properties

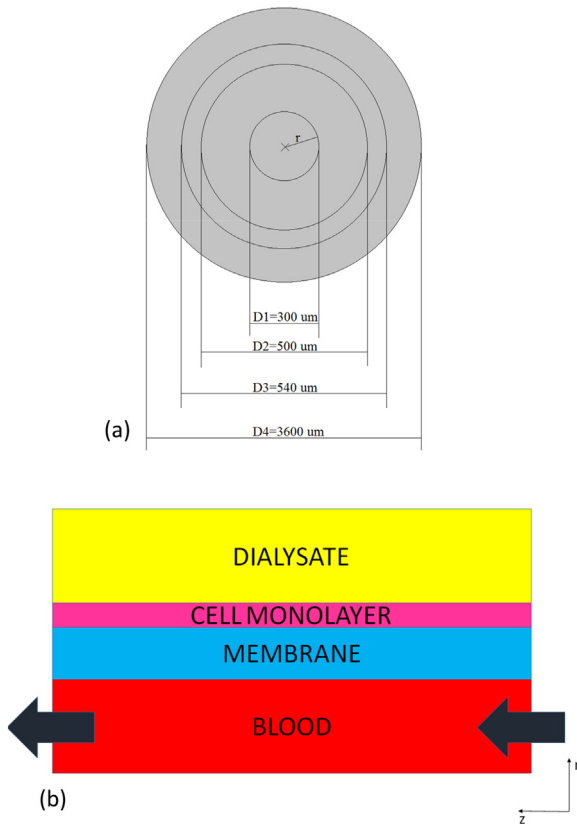


Fig. 1. a) Geometry of the model. D_i represents the external diameter of domain i ($= 1$: blood domain; 2: porous polymeric membrane; 3: cell monolayer; 4: Dialysate). Length of the fiber (normal to the faces shown here) $L = 20$ mm, length of the dialysate domain $L_d = 30$ mm. Hollow fiber lateral area = 0.13 cm^2 , Volume of dialysate = 0.3 mL . b) Configuration of the different domains of the model. Blood domain in the center of the hollow fiber membrane in red, membrane domain in blue, cell monolayer in pink, in contact with the dialysate domain (yellow). (For interpretation of the references to color in this figure legend, the reader is referred to the web version of this article.).

of blood can be used in the model. The blood flows in the longitudinal direction. Toxins are bound to HSA, however, only their free form can be transported through the cells. It is assumed that binding and dissociation kinetics in the blood plasma stream are sufficiently rapid to

allow an equilibrium description of toxin association with and dissociation from albumin in the blood stream.

The transport mechanisms present in this domain are convection in the z direction, and diffusion in the z and r directions. Thus, the relevant transient equations are

$$\frac{\partial C_{i,b}}{\partial t} - D_{i,b} \nabla^2 C_{i,b} + u_{z,b} \nabla C_{i,b} = R_{i,b} \quad (1)$$

where $R_{i,b}$ is the association/dissociation rate for toxin i in blood, $D_{i,b}$ is the diffusivity of toxin i in blood, $C_{i,b}$ is the local concentration of toxin i in blood, and $u_{z,b}$ is the local blood velocity in direction z , defined as

$$u_{z,b}(r) = u_{z,b,max} \left(1 - \left(\frac{r}{R_1} \right)^2 \right) \quad (2)$$

$u_{z,b,max}$ is the maximum velocity in the blood, r is the radial coordinate, and R_1 is the radius of the blood domain, $150 \mu\text{m}$.

In the blood domain, the binding equilibrium constant for toxin i in the presence of HSA is given by

$$k_{eq} = \frac{C_{i,b} C_{HSA,b}}{C_{HSA \cdot i,b}} \quad (3)$$

where $C_{i,b}$, $C_{HSA,b}$, $C_{HSA \cdot i,b}$ are the local concentrations of toxin i , the albumin, and the albumin-toxin complex, respectively. A surface version of the typical Michaelis-Menten expression is assumed on the basolateral side of the cell, where local increase of the dissociation of the albumin-toxin complex is effected by the confinement of albumin molecules at the cell entrance due to steric phenomena, prohibiting their transport into the cell, in combination with the facilitated transport of the toxin molecules thanks to the local action of the transporters, Fig. 2. This local confinement of albumin molecules is expected to affect the diffusion into the porous membrane of the toxin molecules that are detached from the albumin in the vicinity of the basolateral side of the cell. To address this, the diffusivity of the toxin that is produced at the particular site is set to zero within the porous membrane domain. Although this condition increases the sophistication of the model, it is physically compatible with the large increase of the clearance in the presence of albumin compared to the free toxin case.

The leading transport mechanism in the polymer membrane is the diffusion of toxins. Thus, the set of transient equations that describe the domain are

$$\frac{\partial C_{i,m}}{\partial t} - \varepsilon_m D_{i,m} \nabla^2 C_{i,m} = R_{i,m}, \quad (4)$$

where ε_m is the porosity of the membrane, $R_{i,m}$ is the association/

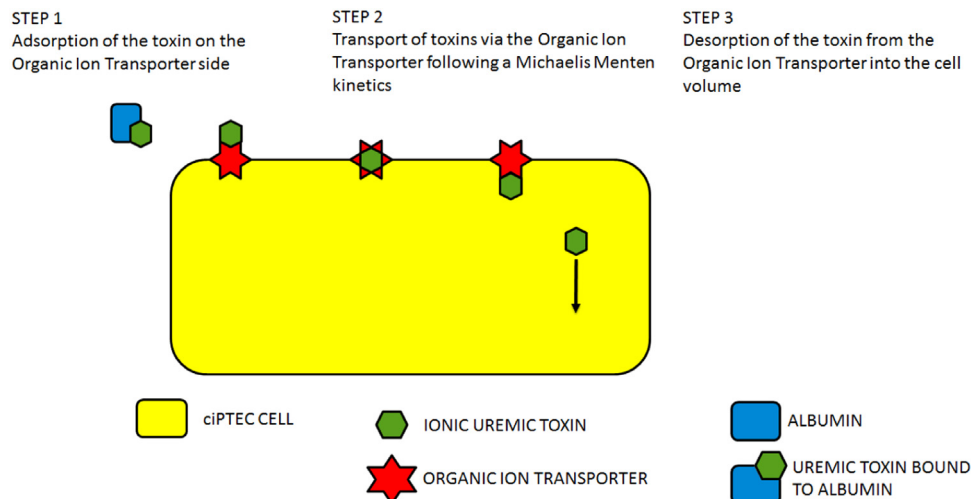


Fig. 2. Action of organic ion transporters. Step 1: Adsorption of protein-bound uremic toxin on the Organic Anion Transporter. Step 2: Transport of toxins via the organic ion transporter following a Michaelis-Menten kinetics. Step 3: Desorption of the toxin from the Organic Anion Transporter.

Table 1

Main transport parameters of the model. The effective diffusivity is estimated as the product of the toxin diffusivity in water with the membrane porosity to tortuosity ratio.

	Blood	Porous layer	Cell monolayer	Dialysate
Indoxyl sulfate effective diffusivity (m ² /s) (25 °C) ^a	5.58309 10 ⁻¹⁰	2.5124 10 ⁻¹⁰	5.58309 10 ⁻¹⁰	5.58309 10 ⁻¹⁰
Flowrate (mL/h) ^b	6	-	-	-
Porosity/Tortuosity (dimensionless) ^c	-	0.45	-	-

^a Diffusivities estimated using Einstein-Stokes equation [21].
^b From experimental conditions [12].
^c Based on typical values for hemodialysis hollow fiber polymeric membranes [23,24].

dissociation rate for toxin *i* in the porous membrane, $D_{i,m}$ is the diffusivity of species *i* in the membrane, and $C_{i,m}$ is the concentration of toxin *i* in the porous membrane. The binding equilibrium constant for toxin *i* in the presence of HSA is the same as the one in the blood, given by Eq. (3).

In the cell monolayer region, cells are assumed to spread throughout the surface, and leave no space between them. The cell monolayer is modeled as a continuous and homogeneous domain. The main transport mechanism within the cell monolayer is intracellular transport; this transport is modeled with a diffusivity constant through the cell monolayer domain, and, in the absence of more accurate information, it is assumed that the diffusivity of toxins inside the cell monolayer is equal to that in water,

$$\frac{\partial C_{i,c}}{\partial t} - D_{i,c} \nabla^2 C_{i,c} = 0 \tag{5}$$

where $D_{i,c}$ is the diffusivity of species *i* (toxin) in the cell monolayer, and $C_{i,c}$ is the concentration of species *i* in the cell monolayer.

The dialysate domain represents the region outside the hollow fiber. The properties of the water are adopted for the dialysate. In this domain, the leading transport mechanism is diffusion in the longitudinal and radial directions. The transport equation that describes this domain is

$$\frac{\partial C_{i,d}}{\partial t} - D_{i,d} \nabla^2 C_{i,d} = 0 \tag{6}$$

where $D_{i,d}$ is the diffusivity of toxin *i* and $C_{i,d}$ is the local concentration of toxin *i* in the dialysate.

The boundary conditions of the model are as follows.
 In the blood domain, along the axial boundary $r = 0$ a symmetry condition is applied,

Table 2

Clearance performance for pure IS transport under various conditions. Experimental clearances from [12].

	ε/τ (dimensionless)	V_{max} (μmol/L min)	Cell diffusivity (m ² /s)	K_m (μmol/L)	Sim. Clearance (μmol/cm ² min)	Exp. Clearance (μmol/cm ² min)
BASE CASE	0.45	5 10 ⁵	5.58 10 ⁻¹⁰	1	43.435	44.00
ET1	0.35	-	-	-	34.174	
ET2	0.25	-	-	-	24.583	
ET3	0.15	-	-	-	14.859	
ET4	0.5	-	-	-	56.587	
VM1	0.45	5 10 ²	-	-	7.117	
VM2	-	5 10 ³	-	-	43.430	
VM3	-	5 10 ⁴	-	-	43.873	
CD1	-	5 10 ⁵	5.58 10 ⁻¹¹	-	39.075	
CD2	-	-	2.79 10 ⁻¹⁰	-	39.245	
CD3	-	-	2.79 10 ⁻¹³	-	15.470	14.08
KM1	-	-	5.58 10 ⁻¹⁰	100	40.485	
KM2	-	-	-	500	31.534	

$$\left(\frac{\partial C_{i,b}}{\partial r}\right)_{r=0} = 0 \tag{7}$$

where $C_{i,b}$ is the concentration of species *i* in the blood domain. The external boundary is at $r = R_1 = 150 \mu\text{m}$, where blood is in contact with the porous membrane, and continuity of fluxes is implemented.

$$-D_{i,b} \left(\frac{\partial C_{i,b}}{\partial r}\right)_{r=R_1} = -D_{i,m} \left(\frac{\partial C_{i,m}}{\partial r}\right)_{r=R_1} \tag{8}$$

$C_{i,b}$ is the concentration of species *i* in the blood domain, $C_{i,m}$ is the concentration of species *i* in the porous membrane, $D_{i,b}$ is the diffusivity of species *i* in the blood domain, and $D_{i,m}$ is the diffusivity of species *i* in the porous membrane.

At the inlet face ($z = 0$) the boundary condition is

$$N_i|_{z=0} = u_{z,b}(r) C_{i,b}|_{z=0} \tag{9}$$

$N_i|_{z=0}$ is the total normal flux of species *i* in the blood domain, $C_{i,b}|_{z=0}$ is the concentration of species *i* in the blood domain at the entrance.

At the outlet ($z = L = 20000 \mu\text{m}$) the diffusive normal flux is considered negligible and the total normal flux of species *i* is their convection flux:

$$-D_{i,b} \left(\frac{\partial C_{i,b}}{\partial z}\right)_{z=L} = 0 \tag{10}$$

In the membrane, the boundary conditions at $z = 0$ and $z = L = 20000 \mu\text{m}$ are the no-flux conditions:

$$-D_{i,m} \left(\frac{\partial C_{i,m}}{\partial z}\right)_{z=\{0,L\}} = 0 \tag{11}$$

At the interface with the cell monolayer ($r = R_2 = 250 \mu\text{m}$), the boundary condition dictates that the diffusive transport of each part of the interface be equal to the Michaelis-Menten uptake rate for the toxin:

$$-D_{i,m} \left(\frac{\partial C_{i,m}}{\partial r}\right)_{r=R_2} = R_{OAT} = -D_{i,c} \left(\frac{\partial C_{i,c}}{\partial r}\right)_{r=R_2} \tag{12a}$$

$$R_{OAT} = \frac{V_{max} C_{i,m} f}{K_m + C_{i,m}} \tag{12b}$$

where V_{max} is the maximum rate, and K_m is the concentration at half-maximum Michaelis-Menten rate in the cell. The surface rate is obtained from its bulk counterpart by the implementation of a form factor *f*, the local volume-to-area ratio at the porous membrane-cell interface.

In the presence of albumin, a similar expression for the rate of dissociation of the albumin-toxin complex is assumed at the porous membrane-cell interface as a boundary condition:

$$R_{i,c} = \frac{V_{max} C_{i,c} f}{K_m + C_{i,c}} \tag{12c}$$

Table 3
Clearance performance of the IS toxin with albumin present in the blood stream under various conditions. Experimental clearances from [12].

	ϵ/τ (dimensionless)	V_{max} ($\mu\text{mol/L min}$)	Cell diffusivity (m^2/s)	K_m ($\mu\text{mol/L}$)	Sim. Clearance ($\mu\text{mol}/\text{cm}^2 \text{ min}$)	Exp. Clearance ($\mu\text{mol}/\text{cm}^2 \text{ min}$)
BASE CASE	0.45	$1 \cdot 10^6$	$5.58 \cdot 10^{-10}$	1	84.347	74.00
ET1	0.35	-	-	-	50.987	
ET2	0.25	-	-	-	48.417	
ET3	0.15	-	-	-	29.536	
ET4	0.5	-	-	-	92.939	
VM1	0.45	$1 \cdot 10^4$	-	-	30.991	
VM2	-	$1 \cdot 10^5$	-	-	64.067	
VM3	-	$1 \cdot 10^7$	-	-	84.000	
CD1	-	$1 \cdot 10^6$	$5.58 \cdot 10^{-11}$	-	84.061	
CD2	-	-	$2.79 \cdot 10^{-10}$	-	84.271	
CD3	-	-	$2.0 \cdot 10^{-13}$	-	0.74	0.81
KM1	-	-	$5.58 \cdot 10^{-10}$	5	84.145	
KM2	-	-	-	10	83.931	
KM3	-	-	-	100	88.442	

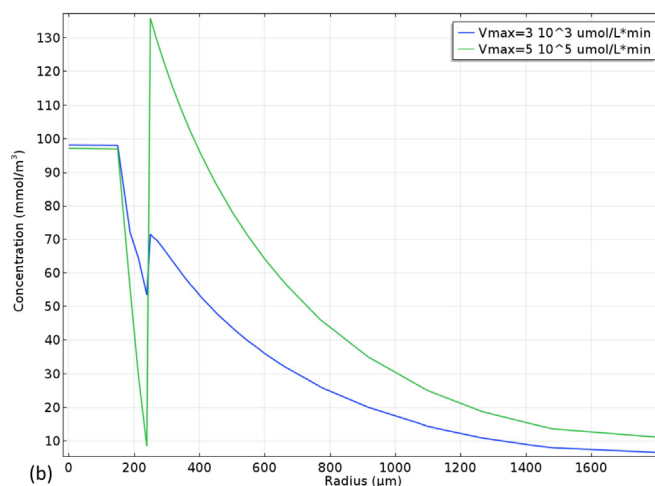
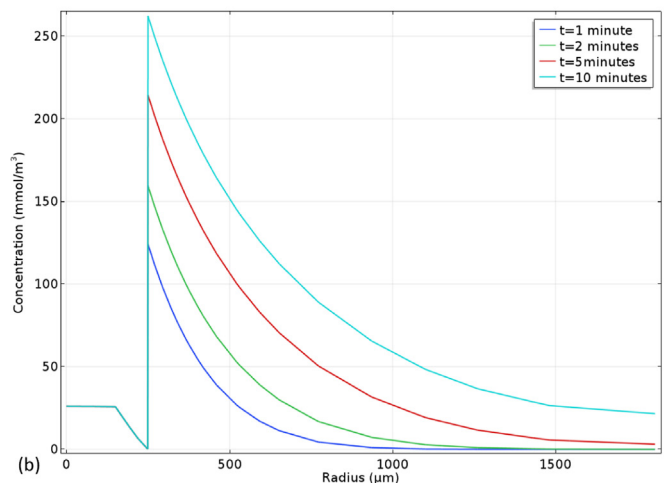
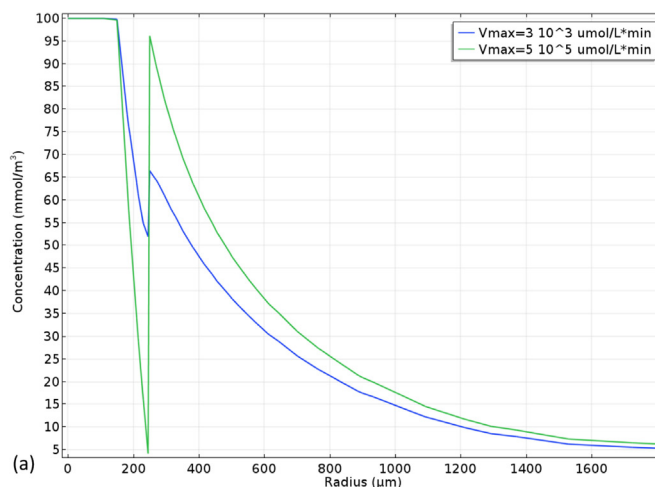
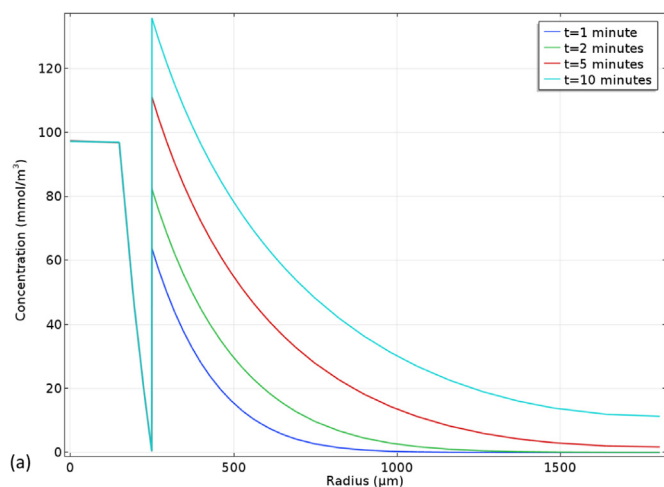


Fig. 3. Evolution of the free indoxyl sulfate concentration profile at $z = 10 \text{ mm}$ in (a) the absence and (b) the presence of albumin.

Note that the concentration of species i may experience a local change across the porous membrane/cell interface just like in the classical dissolution/partitioning model at membrane/bulk interfaces. From the physical point of view, this is attributed to the local action of the transporters, whereas mathematically, this is allowed here thanks to the fact that the two boundary conditions that are imposed are the flux continuity and the Michaelis-Menten dissociation rate, without having to impose any additional constraint to the local concentration. On the other side of the cell, the action of the anti-transporters leads to a delayed discharge of toxin into the apical compartment which, in turn,

Fig. 4. Free indoxyl sulfate concentration profile at $t = 10 \text{ min}$ and (a) $z = 1 \text{ mm}$, (b) $z = 10 \text{ mm}$, in the absence of albumin. Effect of the Michaelis Menten constant, V_{max} .

causes local accumulation of the toxin within the cell domain, next to the basolateral membrane side. Depending on the interplay between the barrier or transport behavior of the basolateral and apical sides of the cell monolayer, local accumulation or depletion of the two cell sides may be noted.

Continuity of fluxes is applied at the outer boundary of the mono-layer domain ($r = R_4 = 270 \mu\text{m}$):

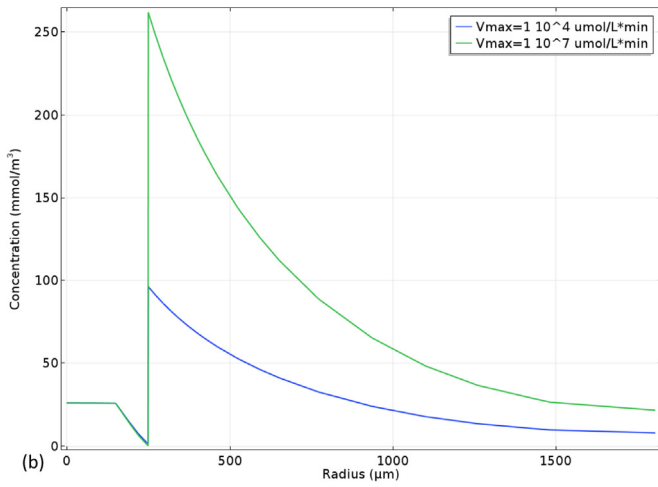
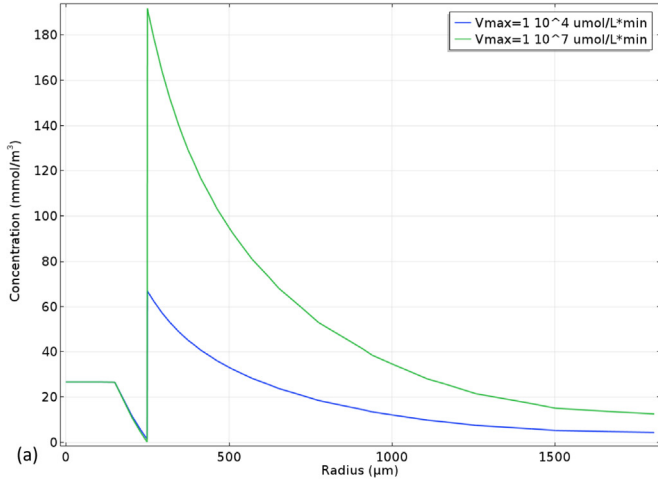


Fig. 5. Free indoxyl sulfate concentration profile at $t = 10$ min and (a) $z = 1$ mm, (b) $z = 10$ mm, in the presence of albumin. Effect of the Michaelis Menten constant, V_{max} .

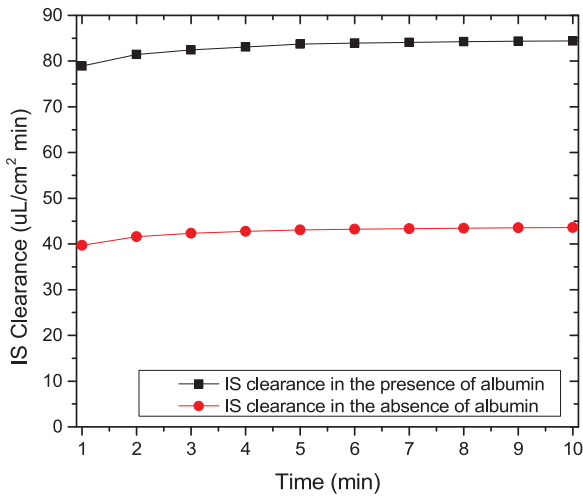


Fig. 6. Indoxyl sulfate clearance vs time in the absence and in the presence of human serum albumin.

$$-D_{i,c} \left(\frac{\partial C_{i,c}}{\partial r} \right)_{r=R_3} = -D_{i,d} \left(\frac{\partial C_{i,d}}{\partial r} \right)_{r=R_3}, \quad (13)$$

The diffusive normal flux is considered negligible at $z = 0$ and



Fig. 7. Experimental indoxyl sulfate clearance (blue, left) vs computer simulation (orange, right) in the absence of albumin. The experimental clearances are reported by Jansen et al. [12]. First column: Cell monolayer. 2nd column: cell monolayer and efflux pump inhibitors. 3rd column: cell monolayer and probocenicid inhibitors.

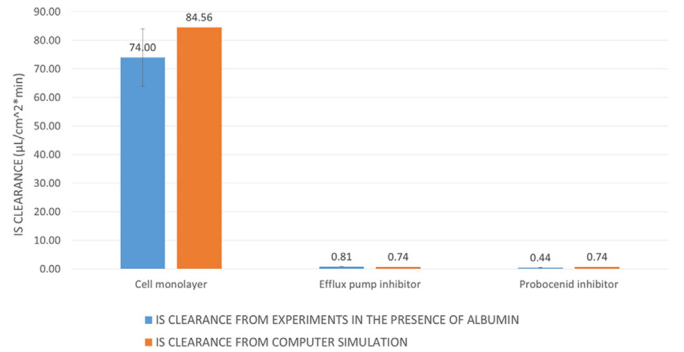


Fig. 8. Experimental indoxyl sulfate clearance (blue, left) vs computer simulation (orange, right) in the presence of albumin. The experimental clearances are reported by Jansen et al. [12]. First column: Cell monolayer. 2nd column: cell monolayer and efflux pump inhibitors. 3rd column: cell monolayer and probocenicid inhibitors.

$z = L = 20000 \mu\text{m}$:

$$-D_{i,c} \left(\frac{\partial C_{i,c}}{\partial z} \right)_{z=\{0,L\}} = 0 \quad (14)$$

Finally, in the dialysate domain, the concentration derivative in the radial direction is negligible ($r = R_4 = 1800 \mu\text{m}$)

$$\left(\frac{\partial C_{i,d}}{\partial r} \right)_{r=R_4} = 0. \quad (15)$$

At $z = 0 \mu\text{m}$ and $z = L_d = 30000 \mu\text{m}$ (the length of the dialysate is larger than that of the fiber), the boundary conditions are zero mass flux for all toxins.

$$N_{i,z=\{0,L_d\}} = 0 \quad (16)$$

3. Parametric analysis

A parametric analysis for the investigation of the role of the unknown critical model parameters has been performed. Numerical solution of the differential equations that were presented in the previous section is achieved by the commercial CFD package COMSOL Multiphysics®. Emphasis is placed on those parameters that are expected to affect significantly the toxin removal predictions, yet their experimental determination is not very practical. These model parameters involve the Michaelis-Menten parameters V_{max} and K_M for the organic ion transporters, the effective toxin diffusivity in the hollow fiber membrane, and the toxin diffusivity inside the cell monolayer.

To facilitate the analysis, two sets of parameters are studied,

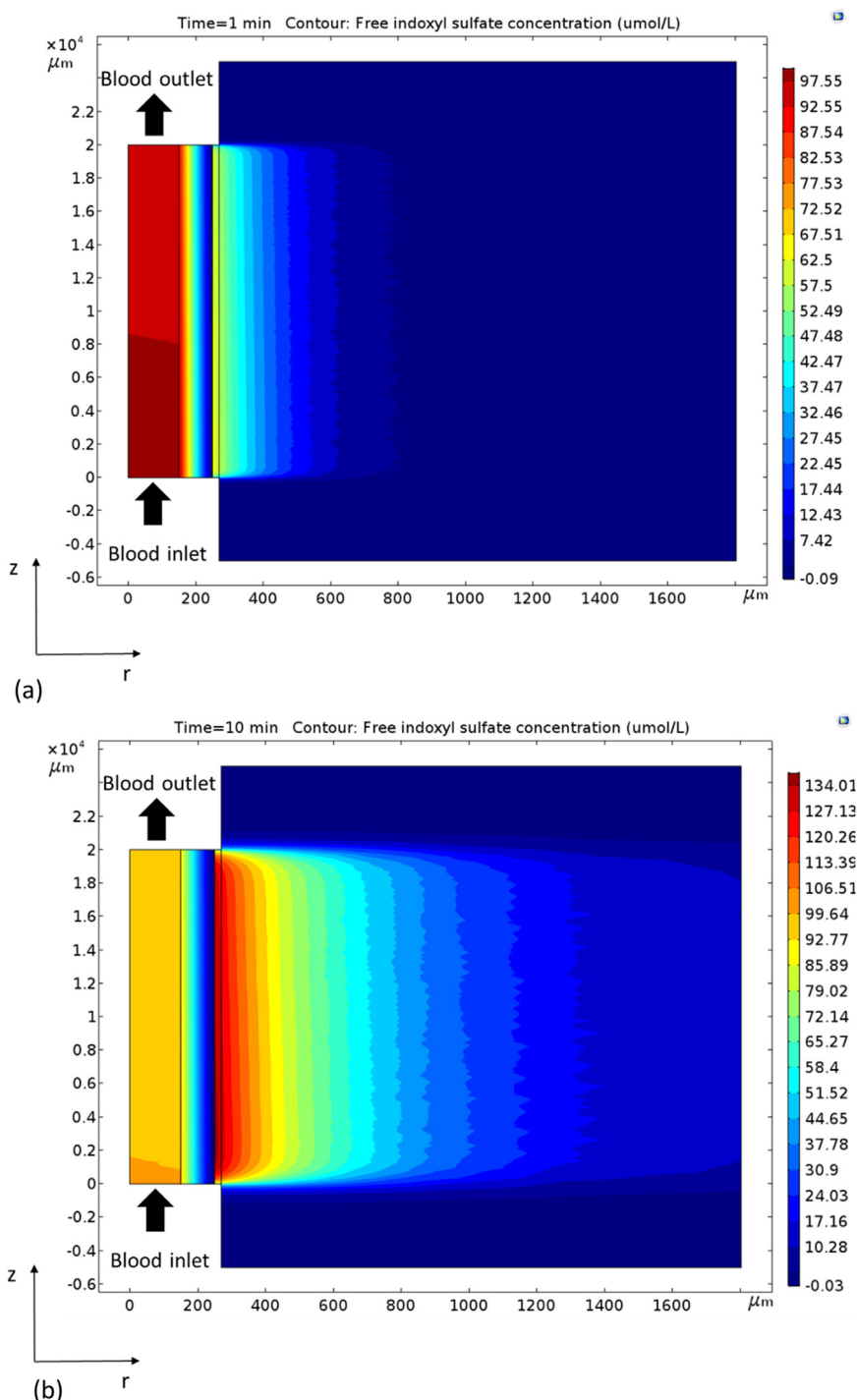


Fig. 9. Contour lines for free indoxyl sulfate concentration in the absence of albumin at (a) 1 min and (b) 10 min.

namely, the Michaelis-Menten kinetics coefficients, and the porous membrane diffusivity coefficients. A list of default parameter and uremic concentration values are given in Tables 1–3, either taken from the literature or determined experimentally.

Toxin diffusivities are calculated using the Einstein-Stokes equation [21], with an estimated radius of 11.10 Å for indoxyl sulfate. Porosity-to-tortuosity values are based on typical values for hemodialysis hollow fiber polymeric membranes [22].

In Table 2, the base case is shown as the specific combination of concentration of organic ion transporters in the form of Michaelis-Menten parameter values for which the model was found to provide the experimental clearance of uremic toxins from the blood. Each and every

parameter was varied while keeping the rest of the parameters constant at their base values.

3.1. Toxin clearance calculations

Experimental indoxyl sulfate clearance curves, expressed in microliters of indoxyl sulfate removed per minute and square centimeter of membrane ($\mu\text{L}/(\text{min cm}^2)$), were provided at different conditions in [12]. More recently, upscaled experiments have been performed under similar conditions [23,24]

The model was adapted to the conditions and geometry of the experiments, and a series of simulations have been performed, using the

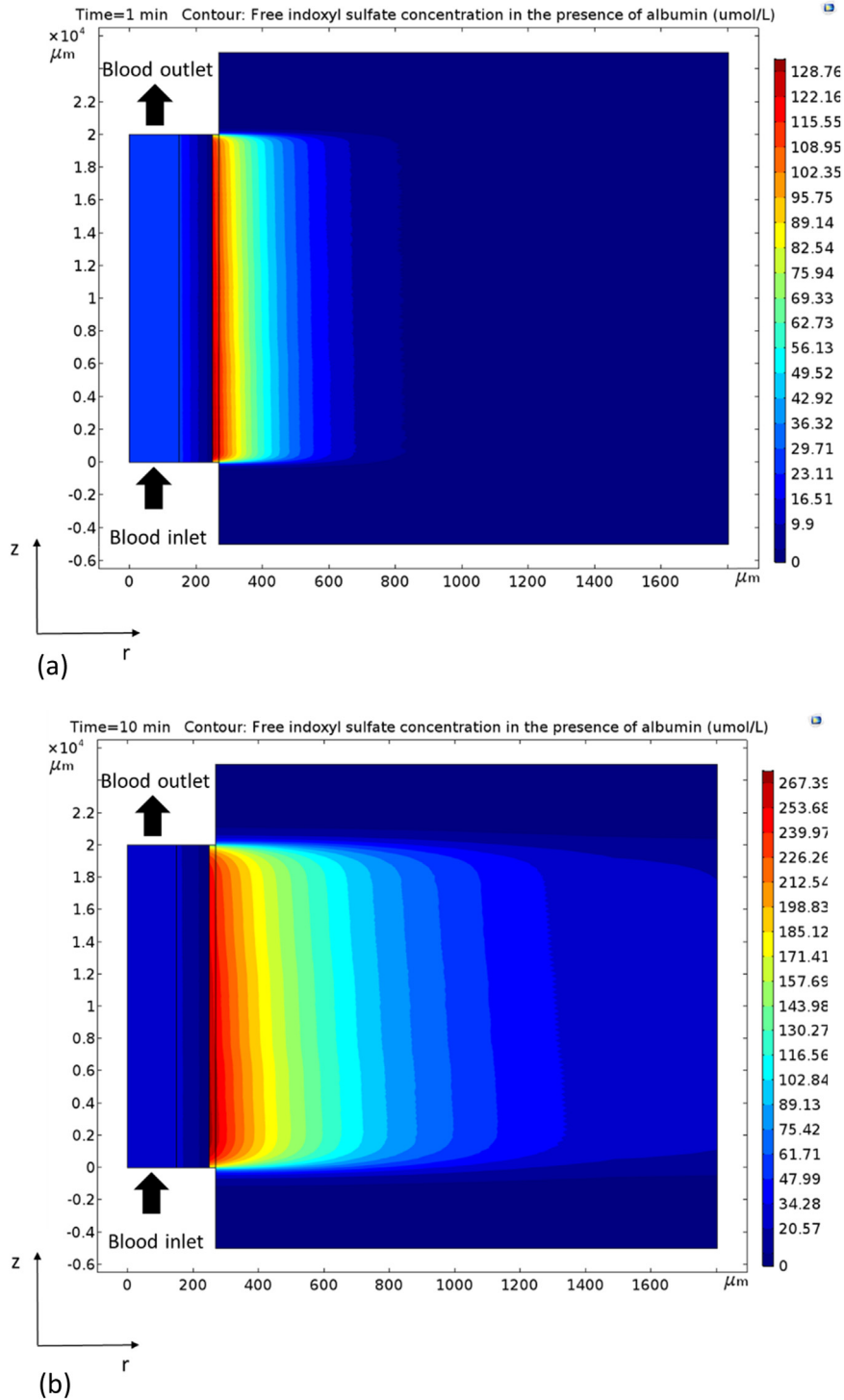


Fig. 10. Contour lines for free indoxyl sulfate concentration in the presence of albumin at (a) 1 min and (b) 10 min.

following definition of clearance [12]

$$Cl_{IS} = \frac{C_{IS,d} V}{C_{IS,b} AT} \quad (17)$$

where $C_{IS,b}$ is the concentration of indoxyl sulfate at the entrance of the blood domain, and $C_{IS,d}$ is the average concentration of indoxyl sulfate at the dialysate domain. A is the lateral area of the hollow fiber membrane, V is the volume of the dialysate compartment, and T is the time of the experiment.

The experimental conditions are as follows: the hollow fiber

membrane is considered homogeneous, the effective length of the fiber is $L = 20$ mm, and the internal and external radii of the membrane are $R_1 = 150$ and $R_2 = 250$ μm , respectively. The effective length of the dialysate domain is larger than that of the fiber, $L_d = 30$ mm, as given by the experimental setup reported in [12].

The blood plasma flow rate is set at $Q = 0.1$ mL/min, which is within the range of the physiological conditions in the kidney and in accordance with the experimental conditions for the sake of comparison between predictions and experiments. Initial conditions (at $t = 0$) for the toxin concentrations include $C_{IS} = C_{IS,0} = 100$ $\mu\text{mol/L}$ at the blood

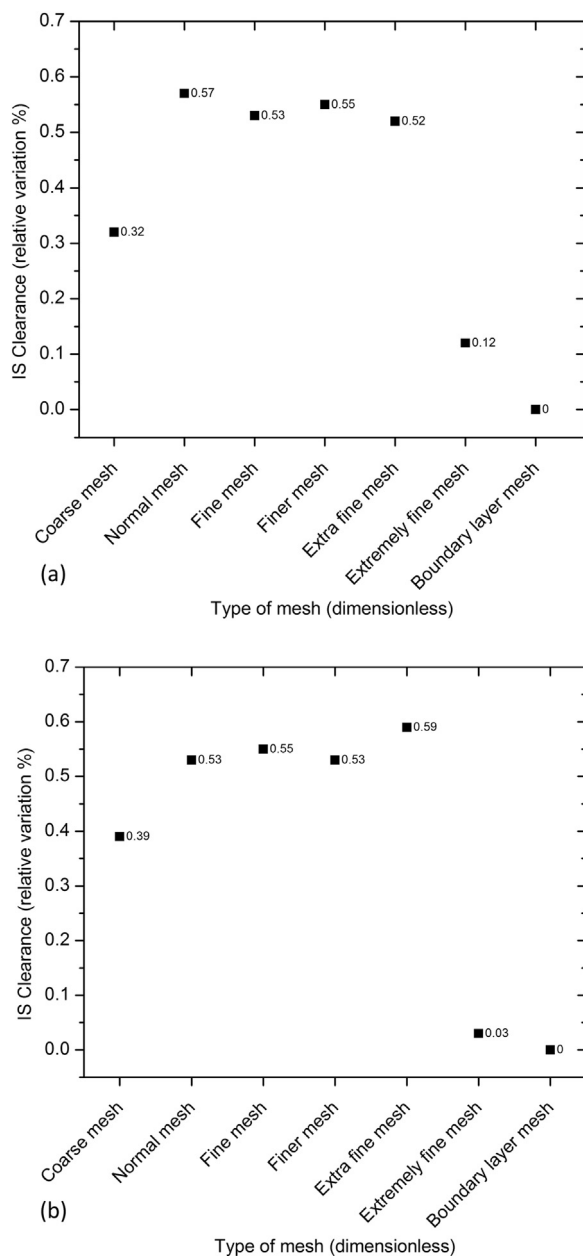


Fig. 11. Relative variation of indoxyl sulfate clearance with different types of mesh, (a) in the absence, and (b) in the presence of albumin.

Table 4

Parameters of the different meshes used in the simulations.

Type of mesh	Type of element	Number of elements	Maximum element size (μm)	Minimum element size (μm)
Coarse	Free triangular	12349	3000	60
Normal	Free triangular	13094	2000	9
Fine	Free triangular	13203	1590	9
Finer	Free triangular	14540	1110	3.75
Extra fine	Free triangular	16487	600	2.25
Extremely fine	Free triangular	28972	300	0.6
Boundary layers ^a	Free triangular and quadratic	67823	600	2.25

^a A series of boundary layers were added in the cell monolayer and at the membrane-cell monolayer interface. Number of boundary layers: 18, type of element in the cell monolayer: quadratic.

stream and the porous medium for the IS in absence of albumin, while $C_{IS} = C_{IS,0} = 100 \mu\text{mol/L}$ for the total (bound plus unbound) IS concentration, and $C = C_{0,\text{albumin},0} = 1000 \mu\text{mol/L}$ for the total (bound plus unbound) albumin concentration, in equilibrium. These are also the inlet concentrations of the IS and the albumin at the inlet face of the blood stream. Zero concentrations are assumed everywhere else initially.

The experiments are performed in four different sets of conditions which were validated through experiments [12]: indoxyl sulfate transport with cell monolayer, and indoxyl sulfate transport with cell monolayer in the presence of an inhibitor of the activity of efflux pumps in the monolayer, while both conditions were carried out in the presence and in the absence of albumin. Variation of key parameters offered numerous modified conditions reported in Tables 2, 3 and used for the parametric investigation of improved BAK designs.

4. Results and discussion

The results of the parametric analysis are presented in this section. It was found that the flux of the uremic toxins through the membrane increased significantly when the transporters are active in the cell monolayer, as expected. The IS concentration in the dialysate is also increased. The sensitivity of the process efficiency to different parameters, such as the effective diffusivity of the porous membrane and the cells, is also investigated.

In all concentration profile figures that follow, the x-axis represents the radial position. Unless otherwise noted, the y-axis represents IS concentration in mmol/m^3 . The results are given at $z = 1 \text{ mm}$ (inlet plane) and at $z = L/2 = 10 \text{ mm}$ (middle plane).

As it was mentioned in Section 2, the adoption of water properties was based on the fact that most of the pertinent experiments, such as in [12], were carried out with an aqueous buffer solution. For comparison purposes, the base case simulations were repeated using the viscosity of the blood keeping all the other parameters constant and assuming constant pressure drop conditions along the fiber length. It was found that the deviation in the prediction of the indoxyl sulfate clearance varied between 10% and 20%.

The temporal evolution of the free IS concentration profile in the absence, as well as in the presence of albumin, at the middle plane ($z = 10 \text{ mm}$), is portrayed in Fig. 3(a),(b). Due to the active transport of IS by the OATs and its gradual accumulation around the cells, the IS concentration is increasing in the stagnant dialysate compartment following a distribution typical to that of diffusion with a source on one side. The absolute values of the concentration in the apical compartment are significantly higher in the case where the albumin is present, Fig. 3(b), compared to the free-toxin-only case, Fig. 3(a), due to the positive effect of the albumin on the clearance performance of the process.

The toxin clearance is affected by the amount of organic ion transporters and BCRP present in the cell monolayer. In the absence of accurate data of concentration of OAT in the cells, the effect of these concentrations is represented in the model by the Michaelis-Menten parameters V_{max} and K_m . The effect of the Michaelis-Menten constant V_{max} on the free indoxyl sulfate concentration profile in the absence of albumin near the inlet ($z = 1 \text{ mm}$) and at half the length of the fiber ($z = 10 \text{ mm}$) for 10 min of operation, is portrayed in Fig. 4(a),(b). Elevated values for V_{max} , the maximum Michaelis-Menten rate, lead to higher fluxes and, thus, higher concentrations in the apical/dialysate part of the system. On the other hand, sufficiently low values of V_{max} have shown a diminishing effect on the flux into the dialysate region (see also Table 2), which may imply that IS transport is due to paracellular transport only.

As expected, the concentration is increased along the length of the fiber in the dialysate part as the toxin is gradually amassed therein. Cases VM1 to VM2 in Table 2 also present the same effect in view of the toxin clearances, however, a limiting threshold in the clearance

performance can be observed there at elevated V_{\max} values, as an order of magnitude increase in the V_{\max} value (VM2 to VM3) does not produce any significant gain in the clearance.

The effect of the Michaelis-Menten constant V_{\max} on the indoxyl sulfate concentration profile at the inlet ($z = 1$ mm) and the middle plane ($z = 10$ mm) for 10 min of operation in the presence of albumin is shown in Fig. 5(a),(b). V_{\max} , by the standard definition in the Michaelis-Menten description, is a reaction rate constant multiplied by the maximum concentration of enzymes, *i.e.*, in the present case the organic ion or the efflux transporters in the cell monolayer. Thus, V_{\max} can be directly increased or decreased by controlling the concentration of the organic ion transporters and the efflux transporters at the basolateral and apical sides of the cell monolayer, respectively. As in the albumin-free case, increased concentration can be observed along the length of the fiber as the toxin is progressively accumulated in the dialysate part. Again, elevated values for V_{\max} , the maximum Michaelis-Menten rate that is provided by the OATs, lead to higher fluxes and, thus, higher concentrations in the apical/dialysate part of the system. The absolute values show an almost two-fold increase of the concentration in the apical compartment, due to the positive effect of the albumin on the clearance performance of the process.

Cases VM1 to VM3 in Table 3 also present the same increasing performance in view of the toxin clearances. The positive presence of the presence of albumin in the effect of the V_{\max} and, thus, the OATs concentrations, is displayed by the extended range of clearances values achieved by ever-increasing the V_{\max} values, in contrast to the no-albumin cases (VM1 to VM3 in Table 2), where a threshold in the clearance can be observed at elevated V_{\max} values.

The aim of the hollow fiber membrane is to offer a support for the cPTEC cell monolayer and to provide the least possible mass resistance to albumin and indoxyl sulfate to facilitate the species to reach the cell monolayer. To this end the effect of the porosity to tortuosity ratio for the membrane, ε/τ , on the free indoxyl sulfate clearance is studied. Clearances after 10 min of operation, in the absence of albumin at different ε/τ , are shown in Table 2, cases ET1-ET4. At increased membrane porosities, the IS toxin has increased effective diffusivities in the vicinity of the cell, which allows increased fluxes of the toxin, providing increased rate of interaction with the OATs of the basolateral wall. This, in turn, provides increased toxin concentrations in the dialysate part, as well as increased clearances. The effect of the porosity to tortuosity ratio of the membrane, ε/τ , on the IS clearances in the presence of albumin is shown in Table 3, cases ET1-ET4. Although the trends are similar to the corresponding ones in the absence of albumin, the absolute values of the concentrations and, thus, of the clearances, are nearly double the ones with no albumin present in the blood stream. The value of *ca.* 80 $\mu\text{L}/\text{cm}^2\text{min}$ is achieved with the base case of Table 3 in accordance to the experimental results [12], portraying the positive effect of the albumin on the toxin clearance. For the BAK device, albumin and the PBUT should be able to reach the cell monolayer without any interaction with the support polymeric membrane. The experimental studies were actually performed using commercial available low fouling membranes used for plasma filtration [12,24]. Besides, due to the relatively short time of the experiments, phenomena that are related to membrane fouling are not considered here.

The fluxes that resulted from the variation of the other parameters follow the respective trends of the concentration distributions, with nearly double clearances compared to the free-toxin cases, Table 2.

Cases CD1 and CD2 correspond to the indoxyl sulfate clearance as the diffusivity of the toxin in the cell monolayer is varied by half an order of magnitude, in the presence and in the absence of albumin (Tables 2, 3, respectively). It is noted that the variation of the cell diffusivity in this range does not affect significantly the indoxyl sulfate clearance.

Parametric analysis for the effect of the Michaelis-Menten constant K_m on the free indoxyl sulfate concentration profile at $z = 10$ mm and $t = 10$ min in the absence of albumin is shown in Table as cases KM1-

KM2. By the typical definition of the Michaelis-Menten kinetics, the K_m values embody the OATs concentration at half-maximum rate ($V_{\max}/2$). Increased K_m values, being in the denominator of the Michaelis-Menten reaction kinetics, seemingly lower the toxin flux permeating the cell through the OAT transport, and the dialysate concentration, as well. This is also evident in cases KM1-KM3 of Table 3, reporting the positive effect of the presence of albumin in the toxin clearance performance of the cells.

The clearances of pure IS for the various parametric calculations that were performed here are provided in Table 2. Clearance of *ca.* 43 $\mu\text{L}/\text{cm}^2$ min is achieved with the base case of Table 2, reproducing quite closely the experimental value reported by [12] for pure IS transcellular transport. The clearance in the presence of albumin, Table 3, are also aligned with experimental findings, and a clearance of *ca.* 84 $\mu\text{L}/\text{cm}^2$ min is obtained with the base case of this configuration. The impeding effect of the presence of inhibitors in the apical part of the cell on the clearance (Cl becomes low, practically diminishing) is modeled by the decrease of the cell diffusivity (case CD3), compared to the no-inhibitors base case (base value). This is true both in the absence, Table 2, and in the presence of albumin, Table 3.

The temporal evolution of the clearance in the absence and in the presence of HSA is portrayed in Fig. 6. The temporal clearance, calculated from the volume integral of the concentration over the apical compartment, that is, the total toxin mass in the dialysate relative to the total toxin mass entered in the blood stream with the time frame of reference, T , Eq. (17), increases with time; however, it reaches a limiting value due to the finite volume of the apical compartment in both cases.

Figs. 7, 8 show the indoxyl sulfate experimental clearance compared with the ones obtained from the models at several conditions. The reported experimental clearances for indoxyl sulfate in the absence of albumin are 44 $\mu\text{L}/\text{cm}^2$ min in the base case, and 14 $\mu\text{L}/\text{cm}^2$ min and 20 $\mu\text{L}/\text{cm}^2$ min in the cases of efflux pump inhibitors and OAT inhibitors, respectively. The model reports indoxyl sulfate clearances of 44 $\mu\text{L}/\text{cm}^2$ min in the base case, and 15 $\mu\text{L}/\text{cm}^2$ min in the cases of inhibitors. In the presence of albumin, the experimental results are 74 $\mu\text{L}/\text{cm}^2$ min for the base case, and 0.8 $\mu\text{L}/\text{cm}^2$ min and 0.4 $\mu\text{L}/\text{cm}^2$ min in the cases of efflux pump and OAT inhibitors, respectively. The corresponding calculated clearance values in the presence of albumin are 85 $\mu\text{L}/\text{cm}^2$ min for the base case, and 0.7 $\mu\text{L}/\text{cm}^2$ min when the effect of inhibitors is implemented.

Figs. 9, 10 show the distribution for free indoxyl sulfate concentration along the fiber at $t = 1$ and $t = 10$ min, in the absence (Fig. 9) and in the presence (Fig. 10) of albumin. In both cases, there is a noticeable increase of free indoxyl sulfate concentration close to the cell monolayer, due to the active role of the organic ion transporters. An increase of indoxyl sulfate concentration in the dialysate domain is observed as time progresses. The levels of free indoxyl sulfate at the blood outlet after 10 min of operation are 93 $\mu\text{mol}/\text{L}$ in the absence of albumin, and 21 $\mu\text{mol}/\text{L}$ in the presence of albumin. It is useful to recall here that the inlet concentrations of free indoxyl sulfate are 100 $\mu\text{mol}/\text{L}$ in the absence of albumin, and 23 $\mu\text{mol}/\text{L}$ in the presence of albumin. The rest of indoxyl sulfate in this case is bound to albumin and it is liberated when the complex albumin-IS reaches the cell monolayer.

Fig. 11(a),(b) show the relative variation of indoxyl sulfate clearance expressed as percentage of the base value, if meshes of different types and resolutions are implemented. The parameters of the mesh used are displayed in Table 4. The most accurate mesh considered here is the “boundary layer” mesh, which involves an extensive series of boundary layers (order of ten) explicitly added in the cell monolayer and at the monolayer interfaces in order to improve the accuracy at the points of action of the organic ion transporters. The indoxyl sulfate clearance varies by up to 0.57% in the absence of albumin, and by up to 0.59% in the presence of albumin when different types of meshes are used. The “boundary layer” mesh gives the most accurate results; however, the computational time is 5 times higher when compared to

the rest of the meshes. Consequently, the mesh that is used to perform the bulk of the simulations is the “extra fine” mesh (see Table 4 for mesh details), which offers a reasonable compromise between accuracy and computational time, and provides results practically as accurate as the “boundary layer” one. The computer used for the simulations has the following specifications: Intel(R) Xeon(R) CPU E5–2620 v3 at 2.40 GHz with 12 cores on 2 sockets. The number of cycles per simulation was 275 in the absence of albumin, and 129 cycles in the simulations where the albumin is present. The average computational time was 120 s in the absence of albumin, and 75 s in the presence of albumin.

5. Conclusions

A multiple domain model of transport and reaction processes was developed for a fiber sample as part of a BAK device, consisting of the blood stream, a porous membrane, a cell monolayer, and a dialysate compartment. Detailed description of the transport, binding/dissociation, and uptake phenomena is provided within the different domains and at the domain interfaces. The model was divided into different domains corresponding to the individual parts of the BAK device, and considered all the relevant transport and reaction mechanisms in each domain. A combined mechanism was implemented to describe the active transport mechanism of organic ion transporters in the cell monolayer, and the role of several important model parameters was quantified, including the Michaelis-Menten kinetic parameters, the porosity-to-tortuosity ratio of the hollow fiber membrane, and the effective diffusivities in the porous membrane and the cell monolayer.

The model offered valuable predictions of uremic toxin transport from blood through a multilayer hollow fiber membrane in the presence of an active cell monolayer at different physiological conditions. At a blood flowrate of 6 mL/h and a concentration of 0.1 $\mu\text{mol/l}$ of total IS, the model predicts a IS clearance of 43 $\mu\text{L}/(\text{min cm}^2)$ in the absence of albumin and a clearance of 84 $\mu\text{L}/(\text{min cm}^2)$ in the presence of 1 $\mu\text{mol/l}$ of human serum albumin. In our model, IS clearance close to zero is predicted when the activity of transporters is inhibited. The above predictions reproduce very closely the experimental data reported in the literature [12,14].

The parametric study concludes that the concentrations of organic ion transporters or, equivalently, the Michaelis-Menten constants, are the most important model parameters affecting the removal of indoxyl sulfate. The effect of the Michaelis-Menten constants simulates the OATs and anti-OATs behavior. Given that their experimental determination is not practical, this parametric analysis offered a quantitative insight on the role of these parameters in the mechanisms of the clearance process of these toxins.

The present model suggests that, in order to achieve higher PBT removal, the rate of transport of PBTs through the polymeric membrane should be maximized using membranes with a higher porosity/tortuosity ratio as stated in cases ET1 to ET4 in Tables 2, 3. In addition, the model predicts that an increase of the V_{max} in the Michaelis-Menten model leads to improved clearance. Given that V_{max} is, by definition, a reaction rate constant multiplied by the concentration of organic ion transporters in the cell monolayer, it is concluded that V_{max} can be increased by increasing the concentration of organic ion transporters and efflux transporters at the basolateral and apical sides of the cell monolayer, respectively. This point can be achieved either by increasing the cell density in the monolayer, or increasing the concentration of transporters in the cells.

In the future, additional transport mechanisms, such as the recovery of electrolytes from the dialysate, the para-cellular transport, and more detailed description of the nature and behavior of the cell monolayer can be included in the model, as well as the scaling-up of the model for several fibers in parallel.

This work sets the first steps in building a functional computational model of a bioartificial kidney device (BAK) and proved that it can

become a valuable tool for the validation and the design of new or improved configurations and guide the design of further experimental strategies.

Acknowledgements

This work was produced as part of the ITN project “TheLink” funded by the European Union's Horizon 2020 Research and Innovation program under the “Marie Skłodowska-Curie” Grant Agreement no. 642890. Methods for transport and sorption simulations in porous membranes were also developed under “Stavros Niarchos Foundation – FORTH Fellowships” within the Greek project ARCHERS.

References

- [1] R. Vanholder, R. de Smet R, N. Lameire, Protein-bound uremic solutes: the forgotten toxins, *Kidney Int.* 59 (Suppl. 78) (2001) S-266–S-270.
- [2] J. Patzer, Principles of bound solute dialysis, *Ther. Apher. Dial.* 10 (2) (2006) 118–124.
- [3] D.A. Buffington, C.J. Pino, C. Lijun, A.J. Westover, G. Hageman, D.H. Humes, Bioartificial renal epithelial cell system (BRECS): a compact, cryopreservable extracorporeal renal replacement device, *Cell Med.* 4 (2012) 33–43.
- [4] D.H. Humes, D. Buffington, A.J. Westover, S. Roy, W.H. Fissell, The Bioartificial kidney: current status and future promise, *Pediatr. Nephrol.* 29 (2014) 343–351.
- [5] N. Diban, D. Stamatialis, Polymeric hollow fiber membranes for bioartificial organs and tissue engineering applications, *Chem. Technol. Biotechnol.* 89 (2014) 633–643.
- [6] J. Jansen, M. Fedecostante, M.J. Wilmer, L.P. van den Heuvel, J.G. Hoenderop, R. Masereeuw, Biotechnological challenges of bioartificial kidney engineering, *Biotechnol. Adv.* 32 (2014) 1317–1327.
- [7] Yar Oo, K. Kandasamy, F. Tasnim, D. Zink, A novel design of bioartificial kidneys with improved cell performance and haemocompatibility, *J. Cell. Mol. Med.* 17 (4) (2013) 497–507.
- [8] Y. Urakami, N. Kimura, M. Okuda, K. Inui, Creatinine transport by basolateral organic cation transporter hOCT2 in the human kidney, *Pharm. Res.* 21 (6) (2004).
- [9] J. Jansen, I.E. De Napoli, M. Fedecostante, C.M.S. Schophuizen, N.V. Chevtchik, M.J. Wilmer, A.H. van Asbeck, H.J. Croes, J.C. Pertsj, J.F.M. Wetzels, L.B. Hilbrands, L.P. Van den Heuvel, J.G. Hoenderop, D. Stamatialis, R. Masereeuw, Human proximal tubule epithelial cells cultured on hollow fibers: living membranes that actively transport organic cations, *Sci. Rep.* 5 (16702) (2015).
- [10] H. Motohashi, Y. Sakurai, H. Saito, S. Masuda, Y. Urakami, M. Goto, A. Fukatsu, O. Ogawa, K. Inui, Gene expression levels and immunolocalization of organic ion transporters in the human kidney, *J. Am. Soc. Nephrol.* 13 (2002) 866–874.
- [11] T. Deguchi, H. Kusuhara, A. Takadate, H. Endou, M. Otogiri, Y. Sugiyama, Characterization of uremic toxin transport by organic anion transporters in the kidney, *Kidney Int.* 65 (2004) 162–174.
- [12] J. Jansen, M. Fedecostante M, M.J. Wilmer, J.G. Peters, U.M. Kreuser, P.H. van den Broek, R.A. Mensik, T.J. Boltje, D. Stamatialis, J.F. Wetzels, L.P. van den Heuvel, J.G. Hoenderop, R. Masereeuw, Bioengineered kidney tubules efficiently excrete uremic toxins, *Sci. Rep.* 6 (26715) (2016).
- [13] M.J. Wilmer, M.S. Saleem, R. Masereeuw, L. Ni, T.J. van der Velden, F. Russel, P.W. Mathieson, L.A. Monnens, L.P. van den Heuvel, E.N. Levchenko, Novel conditionally immortalized human proximal tubule cell line expressing functional influx and efflux transporters, *Cell Tissue Res.* 339 (2010) 449–457.
- [14] J. Jansen, C.M.S. Schophuizen, M.J. Wilmer, S.H.M. Lahham, H.A.M. Mutsaers, J.F.M. Wetzels, R.A. Bank, L.P. van den Heuvel, J.G. Hoenderop, R.A. Masereeuw, A morphological and functional comparison of proximal tubule cell lines established from human urine and kidney tissue, *Exp. Cell Res.* 323 (2014) 87–99.
- [15] M.H. Weissman, T.K. Hung, Numerical simulation of convective diffusion in blood flowing in a channel with a steady, three-dimensional velocity field, *AIChE J.* 17 (1) (1971) 25–30.
- [16] G. Catapano, H.D. Papenfuss, A. Wodetzi, U. Baurmeister, Mass and momentum transport in extra-luminal flow (ELF) membrane devices for blood oxygenation, *J. Membr. Sci.* 184 (2001) 123–135.
- [17] J.B. Papenburg, G.A. Higuera, I.J. de Vries, J. de Boer, C.A. Van Blitterswijk, M. Wessling, D. Stamatialis, Model to design multilayer tissue engineering scaffolds, *Macromol. Symp.* 309/310 (2001) 84–92.
- [18] R. Vanholder, R. de Smet, G. Glorieux, A. Argiles, U. Baurmeister, P. Brunet, W. Clark, G. Cohen, P.P. de Deyn, R. Deppisch, B. Descamps-Latscha, T. Henle, A. Jorres, H.D. Lemke, Z.A. Massy, J. Passlick-Deetjen, M. Rodriguez, B. Stegmayr, P. Stenvinkel, C. Tetta, C. Wanner, W. Zidek, Review on Uremic toxins: classification, concentration and interindividual variability, *Kidney Int.* 63 (2003) 1934–1943.
- [19] S.S. Dukhin, Y. Tabani, R. Lai, O.A. Labib, A.L. Zydnev, M.E. Labib, Outside-in hemofiltration for prolonged operation without clogging, *J. Membr. Sci.* 464 (2014) 173–178.
- [20] T. Sakaki, A. Takadate, M. Otogiri, Characterization of binding site of uremic toxins on human serum albumin, *Biol. Pharm. Bull.* 18 (12) (1995) 1755–1761 (1995).
- [21] C. Cruickshank Miller, The Stokes-Einstein Law for Diffusion in Solution, *Proceedings of the Royal Society, a mathematical, physical and engineering sciences*, Vol. 106, Issue 740, 1924, pp. 724–749.
- [22] W. Baker, *Membrane technology and applications*, Ed. Wiley, 3rd Edition.
- [23] N.V. Chevtchik, M. Mihajlovic, M. Fedecostante, L. Bolhuis-Versteeg, R. Masereeuw, D. Stamatialis, A bioartificial kidney device with polarized secretion of immune modulators, *Tissue Eng. Regen. Med.* (2018), <https://doi.org/10.1002/term.2694>.
- [24] N.V. Chevtchik, M. Fedecostante, J. Jansen, M. Mihajlovic, M. Wilmer, M. R  th, R. Masereeuw, D. Stamatialis, Upscaling of a living membrane for bioartificial kidney device, *Eur. J. Pharmacol.* 790 (2016) 28.